JEMAT 2024, Vol 12, No 2, 83-93
https://doi.org/10.54987/jemat.v12i2.1115

JOURNAL OF ENVIRONMENTAL MICROBIOLOGY AND TOXICOLOGY

Website: http://journal.hibiscuspublisher.com/index.php/JEMAT/index

Isothermal Modeling and MOORA-Guided Model Selection for Hexavalent Chromium Adsorption on a Sugarcane Bagasse–Lemongrass Blend

Aisha Grema[1], Nur Adeela Yasid[1,2], Mohd Ezuan Khayat[1,2], Mohd Badrin Hanizam Abdul Rahim[1,2], Ain Aqilah Basirun[1,2] and Mohd Yunus Shukor[1,2]*

[1]Department of Biochemistry, Faculty of Biotechnology and Biomolecular Sciences, Universiti Putra Malaysia, 43400 UPM, Serdang, Malaysia.
[2]Agribiotechnology Group, Faculty of Biotechnology and Biomolecular Sciences, Universiti Putra Malaysia, UPM 43400 Serdang, Selangor, Malaysia.

*Corresponding author:
Mohd Yunus Shukor,
Department of Biochemistry,
Faculty of Biotechnology and Biomolecular Sciences,
Universiti Putra Malaysia,
43400 UPM,
Serdang,
Malaysia.
Email: mohdyunus@upm.edu.my

HISTORY

Received: 18th Aug 2024
Received in revised form: 24th Nov 2024
Accepted: 22nd Dec 2024

KEYWORDS

Chromium (VI) adsorption
Sugarcane bagasse–lemongrass blend
Isothermal modeling
Nonlinear regression
MOORA ranking

ABSTRACT

Chromium toxicity, present at elevated levels, poses a challenge for its remediation. The use of agricultural spent biomass as an adsorbent is one of the best mitigation efforts to date. This study investigates the adsorption of hexavalent chromium ions (Cr(VI)) onto Sugarcane Bagasse–Lemongrass Blend, and employs nonlinear regression to evaluate several isothermal models. The performance of the models was assessed using multiple error functions. While most models showed good fits, the Koble-Carrigan, Henry, and Dubinin–Radushkevich models showed poor convergence or high error. The Multiobjective Optimization on the Basis of Ratio Analysis (MOORA) method was employed for model ranking, as the error function analysis yielded inconsistent results. MOORA indicated that the Toth, Freundlich, and Fritz–Schlunder III models were the top performers. The Toth model calculated the maximum adsorption capacity of qm_T of 0.91 mg/g, which is slightly lower than the experimental maximum of 1.21 mg/g. The Toth exponent n_T = 0.72 value is closer to unity, suggesting a relatively homogeneous surface with adsorption behavior that resembles the Langmuir model. Despite robust modeling, the limited dataset introduces uncertainty in parameter estimation, underscoring the need for larger datasets. This study also emphasizes MOORA's potential in adsorption science as an efficient multi-criteria model selection tool.

INTRODUCTION

The accelerated growth of industries and mining activities has intensified chromium contamination, largely due to the transformation and circulation of the metal between its trivalent [Cr(III)] and hexavalent [Cr(VI)] states. Of the two, Cr(VI) has a more pronounced toxicity and carcinogenic nature. The predominant applications of chromium in industry is in electroplating, leather tanning, pigment and dye manufacturing, steel production, and metallurgical operations. These industrial sectors are the primary contributors to environmental pollution of chromium, as the mismanagement of industrial waste and unregulated emissions, as well as the discharge of effluents, have resulted in Cr(VI) polluting the surrounding ecosystem [1,2]. The anionic chromate/dichromate species are highly mobile, allowing chromium to migrate and accumulate, posing risks to aquatic life and human health. Chromium pollution is particularly problematic in areas near mining, electroplating, and industrial zones in developing countries [3]. In Malaysia, pollution from chromium is predominantly found in industrial zones, such as leather-processing plants and electroplating activities, where a regulatory gap and infrequent monitoring are the causes of its pollution. The release of chromium into the ecosystem ultimately affects rivers, streams, and sediments. The rural and peri-urban populations are the main zones affected by chromium pollution [3].

This pollution underscores the need for enhanced effluent treatment, regular monitoring to protect ecosystems and public health, and a more comprehensive water quality treatment system [3]. Hexavalent chromium [Cr(VI)] exhibits a strong oxidizing power and the ability to penetrate cellular membranes, which

accounts for its severe toxicity. Cr(VI) is recognized in research as a mutagenic and carcinogenic compound. Its prolonged exposure has been linked to respiratory disorders, renal impairment, and adverse embryonic development [1]. Chromium is essential for modern industry, but at the same time, it is highly hazardous when found at excessive levels in the environment. Hence, this issue has motivated researchers to find better sustainable practices, which include more holistic and advanced treatment technologies. A circular approach is increasingly being used to manage or remediate chromium pollution and waste [2].

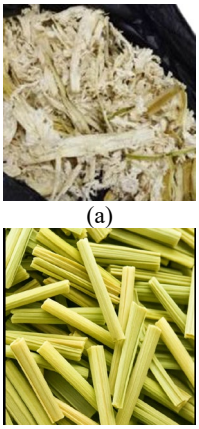

(a) (b)

Fig. 1. Sugarcane bagasse (a) and lemongrass cutting (b) wastes.

Strategies developed to mitigate chromium contamination range from chemical reduction and electrochemical processes to precipitation, ion exchange, and biological approaches. Among these, biosorption is being intensively explored, as it employs natural or engineered biomaterials to remove Cr(VI) from polluted systems. Biosorption is relatively low in operational costs, has minimal energy requirements, and can be regenerated. These attributes make biosorption very appealing, especially for resource-limited regions [4–7]. In addition, biosorption aligns well with the UN's Sustainable Development Goals in preserving ecosystem integrity, reducing waste materials, and is highly scalable [8,9].

In Malaysia, agricultural biomass such as sugarcane bagasse (SB) and lemongrass is increasingly recognized as a highly cost-effective adsorbent for removing xenobiotics, including heavy metals like chromium, from wastewater. Several adsorbents for chromium biosorption using agricultural byproducts have been explored in Malaysia e.g., *Ananas comosus* (AC) peel, *Parkia speciosa* (PS) pods and *Psidium guajava* (PG) peel [10], tea waste (TW), coconut shell (CS), orange peel (OP) [5], rice husk carbon [11], coconut husk [6], sugarcane bagasse [12] and lemongrass [13]. Both lemongrass and sugarcane cultivation are extensively cultivated as agricultural commodities in Malaysia, and the resulting waste biomass is abundantly available and inexpensive to procure, often treated as agricultural waste. This makes both biomass ideal for low-cost environmental remediation strategies via biosorption [12,14–20]. The use of these biomasses in biosorption of pollutants aligns with Malaysia's sustainability goals by valorizing agricultural waste and minimizing landfill use. In this work, the adsorption of chromium on a sugarcane bagasse–lemongrass blend is modeled using various isotherms, and the best model is selected based on a multiobjective optimization analysis.

METHODS

Data acquisition and fitting of isotherm models

Figure 12 data from a previously published study [13] was digitized using the freeware Webplotdigitizer 2.5 [21]. The program's digitization capabilities have garnered accolades for their reliability [22]. Then, Curve-Expert Professional (Version 2.6.5, copyright Daniel Hyams), a program for curve fitting, was used to perform nonlinear regression on the data. MATLAB software package (Mathworks, Massachusetts, USA) was used to resolve the implicit equations. Due to the low number of data points, only models (**Table 1**) with parameters limited to three were deemed appropriate to prevent overfitting.

Table 1. Mathematical models in the remodelling data [23,24].

Isotherm	p	Formula	Ref.
Henry's law	1	$q_e = HC_e$	[25]
Langmuir	2	$q_e = \frac{q_{mL} b_L C_e}{1 + b_L C_e}$	[23]
Jovanovic	2	$q_e = q_{mJ}(1 - e^{-K_J C_e})$	[26]
Freundlich	2	$q_e = K_F C_e^{\frac{1}{n_F}}$	[27]
Dubinin-Radushkevich[a]	2	Incorrect form $q_e = q_{mDR} exp\left\{-K_{DR}\left[RTln\left(1+\frac{1}{C_e}\right)\right]^2\right\}$	[28,29]
		correct form $q_e = q_{mDR} exp\left\{-K_{DR}\left[RTln\left(\left(\frac{C_s}{C_e}\right)\right)\right]^2\right\}$	[30,31]
Koble-Corrigan[c]	3	$q_e = \frac{AC_e^n}{1 + BC_e^n}$	[32]
Temkin[a]	3	$q_e = \frac{RT}{b_T}\{ln(a_T C_e)\}$	[33,34]
Redlich-Peterson	3	$q_e = \frac{K_{RP1} C_e}{1 + K_{RP2} C_e^{\beta_{RP}}}$	[35]
Sips[c]	3	$q_e = \frac{K_s q_{ms} C_e^{\frac{1}{n_S}}}{1 + K_s C_e^{\frac{1}{n_S}}}$	[36]
Toth	3	$q_e = \frac{q_{mT} C_e}{\left(K_T + C_e^{n_T}\right)^{n_T}}$	[37]
Hill[c]	3	$q_e = \frac{q_{mH} C_e^{n_H}}{K_H + C_e^{n_H}}$	[38]
Khan	3	$q_e = \frac{q_{mK} b_K C_e}{(1 + b_K C_e)^{a_K}}$	[39]
BET	3	$q_e = \frac{q_{mBET} \alpha_{BET} C_e}{(1 - \beta_{BET} C_e)(1 - \beta_{BET} C_e + \alpha_{BET} C_e)}$	[40]
Vieth-Sladek	3	$q_e = \frac{q_{mVS} b_{VS} C_e}{(1 + b_{VS} C_e)^{n_{VS}}}$	[41]
Radke-Prausnitz	3	$q_e = \frac{A_{RP} B_{RP} C_e^{\beta}}{A_{RP} + B_{RP} C_e^{\beta - 1}}$	[42–44]
Brouers–Sotolongo	3	$q_e = q_{mBS}\left[1 - \left(1 + (0.5)\left(\frac{t}{\tau}\right)^{\alpha}\right)^{-2}\right]$	[45–47]
Fritz-Schlunder-III	3	$q_e = \frac{q_{mFS} K_{FS} C_e}{1 + K_{FS} C_e^{n_{FS}}}$	[48]
Fowler-Guggenheim[a,b]	3	$q_e = q_{mFG} \frac{K_L C_e e^{\frac{\alpha q_e}{q_{mFG}}}}{1 + K_L C_e e^{\frac{\alpha q_e}{q_{mFG}}}}$	[49]
Moreau	3	$q_e = q_{mM} \frac{bC_e + lb^2 {C_e}^2}{1 + 2bC_e + lb^2 {C_e}^2}$	[50]
Unilan	3	$q_e = \frac{q_{mU}}{2b_U} ln\left(\frac{a_U + C_e e^{b_U}}{a_U + C_e e^{-b_U}}\right)$	

Note

[a]Models that include ln(C_e), implicit equation or any logarithmic function involving C_e will fail or produce NaN (undefined) results when $C_e = 0$. Therefore, data points where $C_e = 0$ should be excluded from the analysis.

[b]Implicit equation or function.

[c]The Hill, Liu (omitted), Sips, and Koble–Corrigan isotherm models will be presented in their traditional forms to preserve their historical context and conceptual distinctions, despite their underlying equality [51,52].

Statistical analysis

This study employed the following statistical discriminatory or error functions tests; HQ (Hannan and Quinn's Criterion) [53], Bias Factor (BF), Accuracy Factor (AF) [54], root-mean-squared error (RMSE), adjusted coefficient of determination (R^2) [55], corrected Akaike Information Criterion (AICc) [56,57], Marquardt's percent standard deviation (MPSD) [58–60] and Bayesian Information Criterion (BIC) [61]. In general, n is the total number of observations, *Obi* and *Pdi* are the predicted and observed values, and p is the total number of parameters of the model [62].

RMSE was calculated using the following formula;

$$RMSE = \sqrt{\frac{\sum_{i=1}^{n}(Pd_i - Ob_i)^2}{n-p}} \quad \text{(Eqn. 1)}$$

BF and AF were calculated using the following formula;

$$Bias\ factor = 10\left(\sum_{i=1}^{n} log\frac{(Pd_i/Ob_i)}{n}\right) \quad \text{(Eqn. 2)}$$

$$Accuracy\ factor = 10\left(\sum_{i=1}^{n} log\frac{|(Pd_i/Ob_i)|}{n}\right) \quad \text{(Eqn. 3)}$$

AICc was calculated using the following formula;

$$AICc = 2p + n\ln\left(\frac{RSS}{n}\right) + \frac{2(p+1)+2(p+2)}{n-p-2} \quad \text{(Eqn. 4)}$$

BIC was calculated using the following formula;

$$BIC = n\ln\left(\frac{RSS}{n}\right) + k\ln(n) \quad \text{(Eqn. 5)}$$

HQC was calculated using the following formula;

$$HQC = nIn\left(\frac{RSS}{n}\right) + 2k\ln(\ln n) \quad \text{(Eqn. 6)}$$

Adjusted coefficient of determination (R^2) was calculated using the following formula;

$$Adjusted\ (R^2) = 1 - \frac{RMS}{S_Y^2} \quad \text{(Eqn. 7)}$$

$$Adjusted\ (R^2) = 1 - \frac{(1-R^2)(n-1)}{(n-p-1)} \quad \text{(Eqn. 8)}$$

MPSD was calculated using the following formula;

$$MPSD = 100\sqrt{\frac{1}{n-p}\sum_{i=1}^{n}\left(\frac{Ob_i - Pd_i}{Ob_i}\right)^2} \quad \text{(Eqn. 9)}$$

Application of Multiobjective Optimization by Ratio Analysis (MOORA) in Modeling

MOORA, or Multiobjective Optimization by Ratio Analysis, is a multi-criteria decision-making (MCDM) method for ranking models. MOORA identifies the optimal model by simultaneously evaluating multiple performance metrics [63, . In MOORA, the normalization of the decision matrix is the first step to ensure comparability among different performance metrics. Normalization uses the following equation:

$$X'_{ij} = \frac{X_{ij}}{\sqrt{\sum_{i=1}^{n} X_{ij}^2}} \quad \text{(Eqn. 10)}$$

Where X_{ij} is the original value of the j^{th} metric for the i^{th} model, and X'_{ij} is the normalized value**.**

Ratio System Analysis

The aggregation of the normalized values was then carried out using a ratio system approach. Summation of the beneficial criteria (those that should be maximized, $adjR^2$) is subtracted from the summation of non-beneficial criteria (the rest of the error functions) using the following formula:

$$Y_i = \sum_{beneficial} X'_{ij} - \sum_{non-beneficial} X'_{ij} \quad \text{(Eqn. 11)}$$

Where Y_i is the final score for the i^{th} model

If a particular evaluation criterion is found to be more significant than others, weighted ratios can be introduced to the analysis. Nevertheless, in this study, the approach of weighting was not used since no clear consensus exists in the literature regarding the relative importance of the error functions being assessed. The procedure thus ranks models according to their overall performance scores, where a higher score indicates better predictive capability. The top score model was deemed the most suitable under the defined decision framework. A fair and transparent comparison of kinetic models is achieved using this structured approach. This approach enables multiple assessment metrics to be incorporated in the identification of the best model.

RESULTS AND DISCUSSION

The fitting of various isotherm models to the equilibrium data of the adsorption isotherm of Cr (VI) using a blend derived from sugarcane bagasse and lemongrass [13], as determined by nonlinear regression, is shown in **Figs**. **2–21**. The results showed that all these models provided good data fits, except for the Koble-Carrigan, Henry, and Dubinin–Radushkevich models. The error function analysis showed that the Toth model was the most frequently selected as the best model, as shown in **Table 2.** To further confirm this, the Multiobjective Optimization on the Basis of Ratio Analysis (MOORA) method was applied. MOORA systematically evaluates and ranks the performance of the adsorption isotherm models (**Table 3**). As expected, the MOORA scores indicated that the Toth model was the best with a score of 1.0396, reinforcing the earlier error function analysis.

The Toth equation effectively explains the heterogeneity and Langmuir-type behavior of the system. The second best was the Freundlich with a score of 0.7387). This is followed by the Fritz–Schlunder III model in third place with a score of 0.7331. Despite this, its very large confidence interval values in earlier fits highlight potential limitations in reliability despite its competitive MOORA score. The Radke–Prausnitz and Khan models occupied the fourth and fifth positions, respectively, with a close performance, having scores of nearly 0.731. The Redlich–Peterson model ranked sixth. In the mid-range, models such as Brouers–Sotolongo were 7th, Vieth–Sladek were 8th, and Sips and Hill were tied at 9th due to the reason explained. In these models, having the same rank, the Standard Competition Order (SCO) ranking method was then applied, where the subsequent rank was skipped [52]. In the original study on Cr (VI) adsorption onto a sugarcane bagasse–lemongrass blend [13], the Freundlich model was found to be a better fit than the Langmuir model based on the error function R^2 and χ^2.

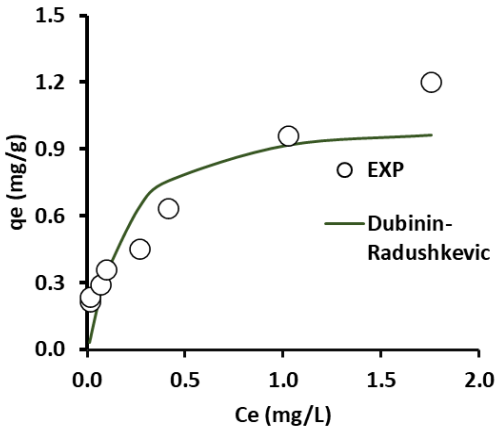

Fig. 2. Cr (VI) adsorption onto sugarcane bagasse–lemongrass blend modelled using the Dubinin-Radushkevic model.

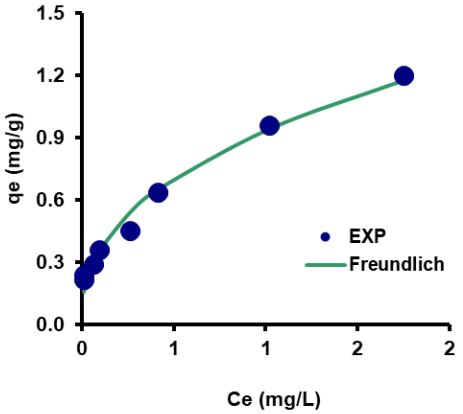

Fig. 5. Cr (VI) adsorption onto sugarcane bagasse–lemongrass blend modelled using the Freundlich isotherm model.

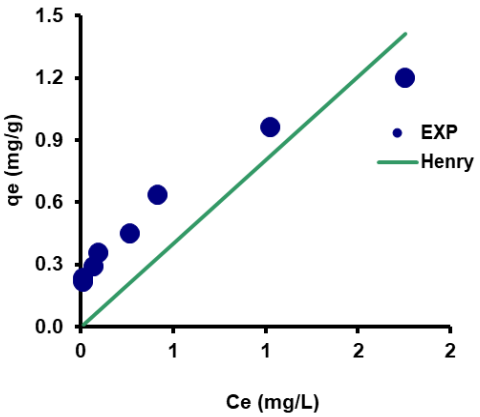

Fig. 3. Cr (VI) adsorption onto sugarcane bagasse–lemongrass blend modelled using the Henry model.

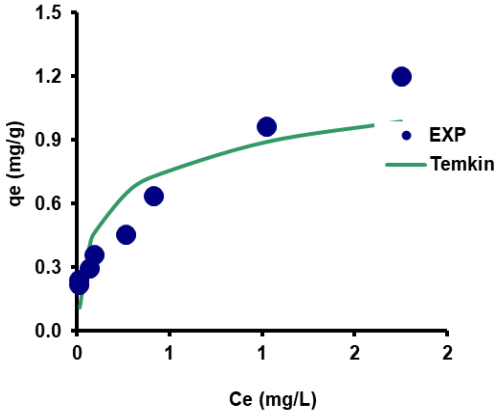

Fig. 6. Cr (VI) adsorption onto sugarcane bagasse–lemongrass blend modelled using the Temkin isotherm model.

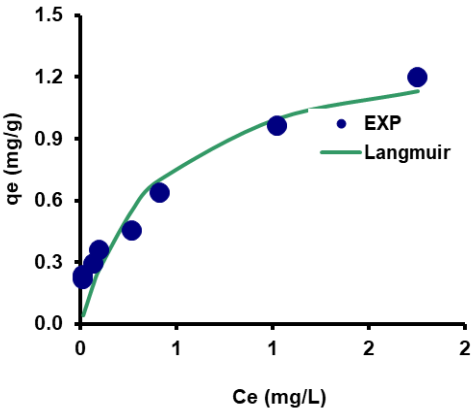

Fig. 4. Cr (VI) adsorption onto sugarcane bagasse–lemongrass blend modelled using the Langmuir isotherm model.

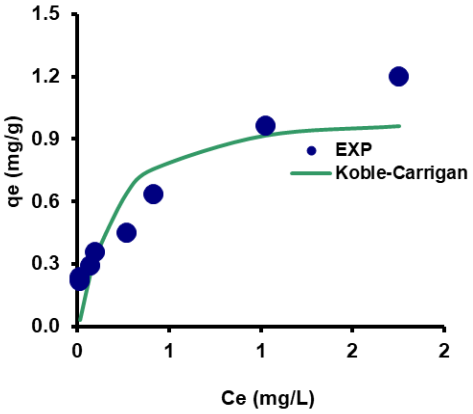

Fig. 7. Cr (VI) adsorption onto sugarcane bagasse–lemongrass blend modelled using the Koble-Corrigan isotherm model.

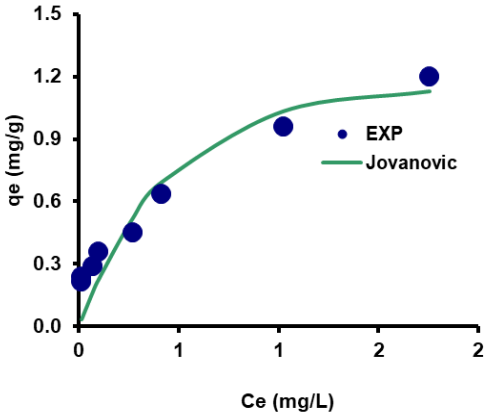

Fig. 8. Cr (VI) adsorption onto sugarcane bagasse–lemongrass blend modelled using the Jovanovic isotherm model.

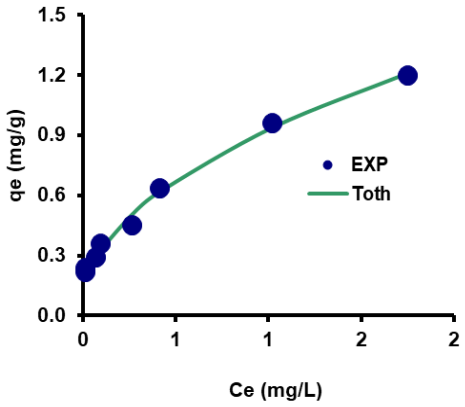

Fig. 11. Cr (VI) adsorption onto sugarcane bagasse–lemongrass blend modelled using the Toth isotherm model.

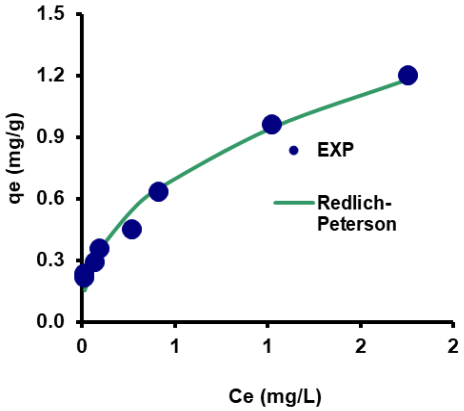

Fig. 9. Cr (VI) adsorption onto sugarcane bagasse–lemongrass blend modelled using the Redlich-Peterson isotherm model.

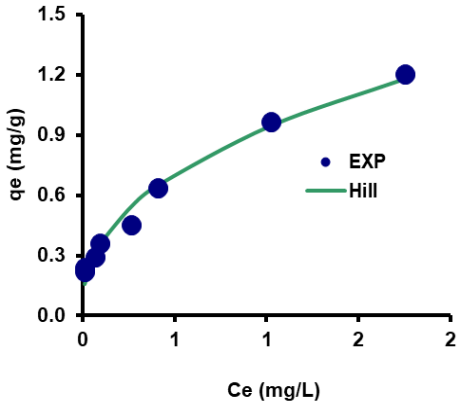

Fig. 12. Cr (VI) adsorption onto sugarcane bagasse–lemongrass blend modelled using the Hill isotherm model.

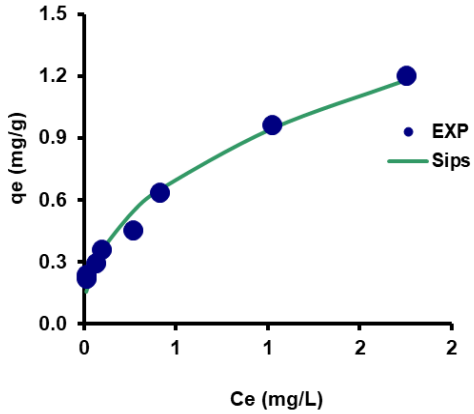

Fig. 10. Cr (VI) adsorption onto sugarcane bagasse–lemongrass blend modelled using the Sips isotherm model.

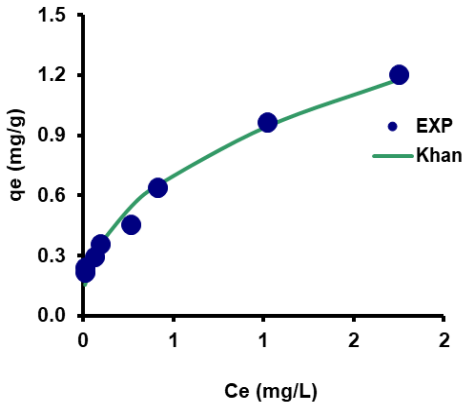

Fig. 13. Cr (VI) adsorption onto sugarcane bagasse–lemongrass blend modelled using the Khan isotherm model.

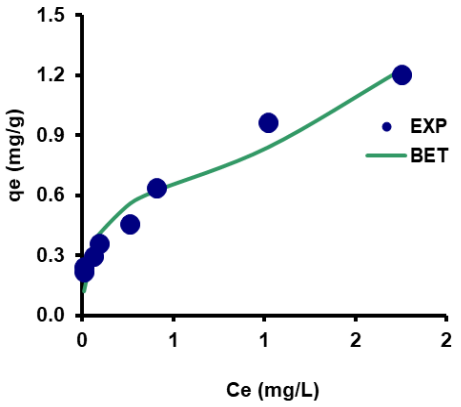

Fig. 14. Cr (VI) adsorption onto sugarcane bagasse–lemongrass blend modelled using the BET isotherm model.

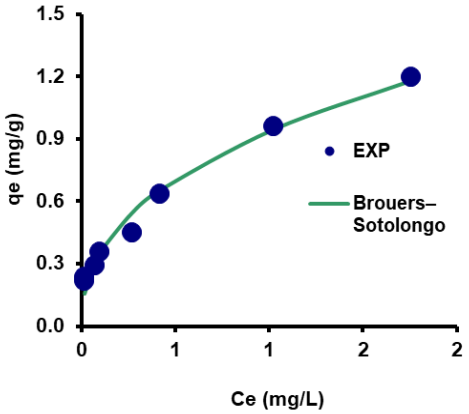

Fig. 17. Cr (VI) adsorption onto sugarcane bagasse–lemongrass blend modelled using the Brouers-Sotolongo isotherm model.

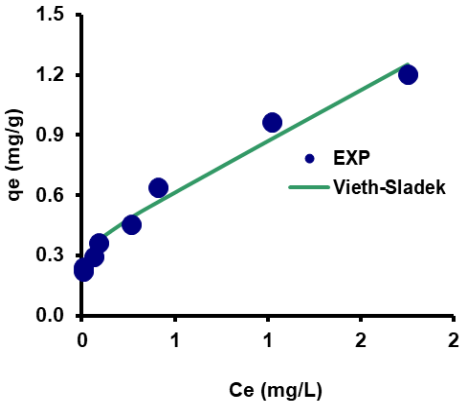

Fig. 15. Cr (VI) adsorption onto sugarcane bagasse–lemongrass blend modelled using the Vieth-Sladek isotherm model.

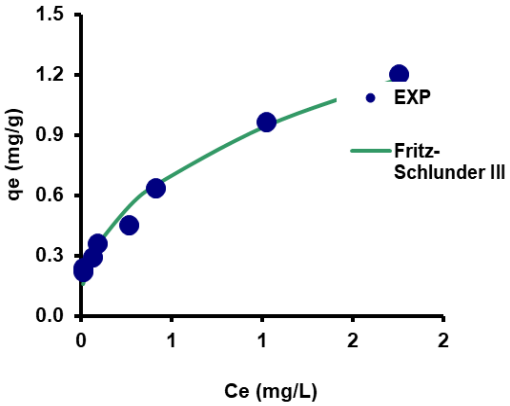

Fig. 18. Cr (VI) adsorption onto sugarcane bagasse–lemongrass blend modelled using the Fritz-Schlunder III isotherm model.

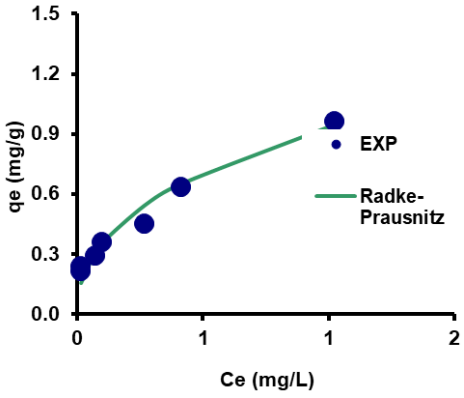

Fig. 16. Cr (VI) adsorption onto sugarcane bagasse–lemongrass blend modelled using the Radke-Prausnitz isotherm model.

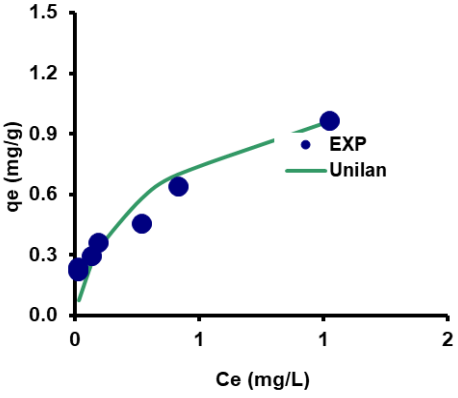

Fig. 19. Cr (VI) adsorption onto sugarcane bagasse–lemongrass blend modelled using the Unilan isotherm model.

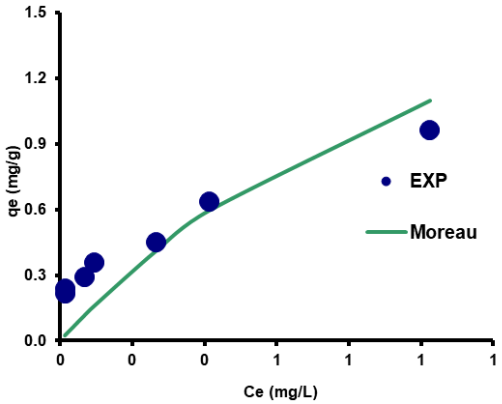

Fig. 20. Cr (VI) adsorption onto sugarcane bagasse–lemongrass blend modelled using the Moreau isotherm model.

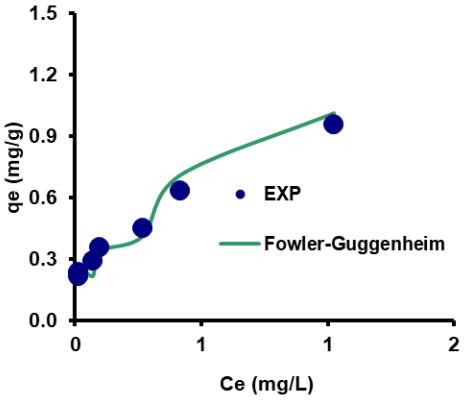

Fig. 21. Cr (VI) adsorption onto sugarcane bagasse–lemongrass blend modelled using the Fowler-Guggenheim isotherm model.

Table 2. Error function analysis for the fitting of the isotherm of Cr (VI) adsorption onto sugarcane bagasse–lemongrass blend.

	Model	*p*	MPSD	RMSE	R^2	adR^2	AICc	BIC	HQC	BF	AF
1	Henry	1	197.32	0.252	0.75	0.707	-14.745	-21.07	-21.68	0.563	1.851
2	Langmuir	2	26.58	0.133	0.92	0.881	-18.587	-30.43	-31.66	0.950	1.145
3	Freundlich	2	77.34	0.057	0.98	0.972	-32.076	-43.92	-45.15	1.027	1.039
4	Temkin	3	29.12	0.173	0.80	0.658	-4.497	-25.59	-27.44	1.109	1.186
5	Koble-Carrigan	2	315.29	0.177	-16.59	-23.63	-14.000	-25.84	-27.07	1.001	1.138
6	Jovanovic	2	10.56	0.147	0.90	0.864	-16.959	-28.80	-30.03	0.898	1.196
7	Redlich-Peterson	3	9.77	0.064	0.98	0.963	-20.477	-41.57	-43.42	1.027	1.039
8	Sips	3	21.51	0.063	0.98	0.964	-20.742	-41.84	-43.68	1.027	1.039
9	Toth	3	9.72	0.032	0.99	0.990	-31.524	-52.62	-54.47	0.999	1.033
10	Hill	3	21.51	0.063	0.98	0.964	-20.742	-41.84	-43.68	1.027	1.039
11	Khan	3	9.94	0.063	0.98	0.964	-20.689	-41.78	-43.63	1.028	1.039
12	BET	3	173.39	0.106	0.94	0.900	-12.342	-33.44	-35.28	1.049	1.090
13	Vieth-Sladek	3	9.94	0.063	0.98	0.961	-20.578	-41.67	-43.52	1.022	1.074
14	Radke-Prausnitz	3	9.94	0.063	0.98	0.964	-20.693	-41.79	-43.63	1.028	1.039
15	Brouers–Sotolongo	3	11.16	0.063	0.98	0.964	-20.539	-41.63	-43.48	1.028	1.039
16	Fritz-Schlunder III	3	9.78	0.063	0.98	0.964	-20.742	-41.84	-43.68	1.027	1.039
17	Unilan	3	29.61	0.122	0.93	0.881	-10.038	-31.13	-32.98	1.016	1.073
18	Fowler-Guggenheim	3	54.58	0.063	0.98	0.965	-20.580	-41.68	-43.52	0.959	0.959
19	Moreau	3	39.34	0.189	0.88	0.793	-3.078	-24.17	-26.02	0.797	0.797
20	Dubinin-Radushkevic	2	17.71	0.18	0.81	0.74	-14.00	-25.84	-27.07	1.00	1.14

Note:
RMSE Root mean Square Error
adR^2 Adjusted Coefficient of determination
p no of parameters
AF Accuracy factor
BF Bias factor
BIC Bayesian Information Criterion
AICc Adjusted Akaike Information Criterion
HQC Hannan–Quinn information criterion

Table 3. Ranking of isothermal models based on MOORA.

No	Model	MOORA Score	Rank
1	Toth	1.03960	1
2	Freundlich	0.73865	2
3	Fritz-Schlunder III	0.73312	3
4	Radke-Prausnitz	0.73121	4
5	Khan	0.73111	5
6	Redlich-Peterson	0.72479	6
7	Brouers–Sotolongo	0.72356	7
8	Vieth-Sladek	0.71921	8
9	Sips	0.70571	9
10	Hill	0.70571	9
11	Fowler-Guggenheim	0.62407	11
12	Langmuir	0.35491	12
13	Unilan	0.31011	13
14	Jovanovic	0.30446	14
15	Dubinin-Radushkevic	0.18800	15
16	Temkin	0.06995	16
17	BET	0.06418	17
18	Moreau	0.00054	18
19	Henry	-0.66699	19
20	Koble-Carrigan	-2.54	20

Isothermal Modeling of Cr(VI) Adsorption

The Toth model calculated the maximum adsorption capacity of qm_T of 0.91 mg/g. This value is lower than the experimental maximum of 1.21 mg/g. The confidence interval of 0.866–0.956 mg/g was narrow, confirming that this underestimation is consistent across the model. Furthermore, the Toth exponent n_T = 0.72 (95% CI: 0.675–0.765) value is closer to unity, suggesting a relatively homogeneous surface with adsorption behavior that resembles the Langmuir model. The Freundlich model, in contrast, yielded a comparable adsorption capacity estimate (qmF = 1.179 mg/g) and a Freundlich constant (KF = 0.94), with nF = 2.43. The high value of n_F (>1) points to favorable adsorption and moderate surface heterogeneity. The Fritz–Schlunder III model returned a maximum adsorption capacity of 0.94 mg/g; however, the fitted equilibrium constant KF was very large (6.27 × 10^8), suggesting instability and poor reliability of the model. The exponent n_{FS} = 0.59 (95% CI: 0.491–0.685) suggests suboptimal fitting when compared with Freundlich or Langmuir models.

The Langmuir model aligned well with the experimental maximum, with the predicted highest capacity at 1.39 mg/g (95% CI: 0.838–1.947 mg/g). This value supports the hypothesis of monolayer adsorption on a relatively homogeneous set of active sites. The Langmuir constant k_L = 2.46 L/mg showed a wide confidence interval (−0.185 to 5.108), which suggests a moderate affinity between Cr(VI) ions and the sugarcane bagasse–lemongrass surface if the model is true. The Toth model underpredicts adsorption capacity but trends toward Langmuir-type behavior. The Fritz–Schlunder III appears unsuitable for this dataset. In this study, the limited number of data points (<10) constrains statistical reliability, although the fits remain within the range which is typically reported in adsorption research.

Table 4. Isothermal models' constants for Cr(VI) adsorption onto a sugarcane bagasse–lemongrass blend.

Model	Para-meter	Unit	Value	[13] value	95% CI
Toth	q_{mT}	(mg g^{-1})	0.91		0.866 to 0.956
	K_T	(mg/L)^{nT}	-0.03		-0.04 to -0.01
	n_T		0.72		0.675 to 0.765
Freundlich isotherm	K_F	(mg g^{-1}.L mg^{-1})$^{1/n}$	0.94	0.9237	0.859 to 1.012
	n_F	(L mg^{-1})	2.43	0.4246	1.973 to 2.887
	q_{mF} *	mg g^{-1}	1.179		
Fritz-Schlunder III	q_{mFS}	mg g^{-1}	0.94		0.838 to 1.034
	K_{FS}		627149475.2		Too large
	nF_S		0.59		0.491 to 0.685
Langmuir	Qm_S	(mg/g)	1.39	1.4397	0.838 to 1.947
	k_L	(L/mg)	2.46	2.1289	-0.185 to 5.108

*Estimated using the Halsey rearrangement.

In the assessment of Cr(VI) adsorption by diverse agricultural biomasses via sorption capacity measurements and isotherm model selection, the results indicated substantial disparities among the agricultural biomass materials (**Table 5**). The Langmuir model was the best fit for nearly all agricultural biomasses, such as sorghum stem powder and casuarina fruit powder, which had low sorption capacities of 0.68 mg/g and 0.70 mg/g, respectively [63]. It is likely that these adsorbents exhibit low Qm values due to their small surface area and likely few active functional groups for interacting with chromium ions.

The Freundlich and Toth models are the most suitable models for dried water hyacinth root and sugarcane bagasse–lemongrass blends, which can adsorb 1.28 mg/g and 1.44 mg/g, respectively. The low values indicate that they have only a moderate potential for use. This remodelling study showed that the Toth model exhibited a more accurate fit for the adsorption data than the Langmuir and the Freundlich models. For the typical agricultural biomass, the Toth model more accurately depicts biosorbent surfaces that are likely to be heterogeneously distributed. The binding sites within the sugarcane bagasse–lemongrass composite can vary due to differences in experimental design, different sub-species, preparation methods, blending ratios, and particle sizes, which may have led to a lower Q_m value compared to earlier Langmuir-based findings [13]. The adsorption performance of olive leaves pruning waste and chemically modified teff straw was best modelled using the Langmuir model with Q_m values of 3.90 mg/g and 5.10 mg/g, respectively [64,65]. Surface modification techniques may generate additional active sites, leading to improved sorption results.

The Langmuir model was also utilized in modelling the adsorption behavior of soy hull, with a maximum adsorption capacity of 7.29 mg/g (Blanes et al., 2016). The high porosity and numerous hydroxyl and carboxyl functional groups in soy hulls likely facilitate strong electrostatic bonding with Cr(VI), thereby enhancing its adsorption capacity.

The research findings indicate that basic agro-wastes such as sorghum and casuarina fruit possess minimal adsorption capacity, whereas soy hull, olive leaves, and modified teff straw exhibit significantly enhanced potential as adsorbents. The research substantiates that sugarcane bagasse–lemongrass composites serve as economical biosorbents, despite exhibiting lower Qm values compared to alternative materials. Additionally, the Toth model offers a a superior representation of the system's heterogeneity. The results show that blended biomasses require additional chemical or physical modifications to enhance their ability to adsorb, ultimately reaching levels comparable to those of high-performance materials.

Table 5. Comparison of agricultural biomass adsorbents for Cr(VI) removal, highlighting the best-fitting isotherm models, maximum adsorption capacities (Qm), and relevant literature references.

Agriculture biomass	Best isotherm model	Cr (VI) Qm (mg/g)	Ref
Sorghum stem powder	Langmuir	0.68	[63]
Casuarinas fruit powder	Langmuir	0.70	[63]
Dried water hyacinth root (DWHR)	Freundlich	1.28	[66]
Olive leaves Chemlali pruning waste (OLC)	Langmuir	3.90	[64]
Teff straw-based	Langmuir	5.10	[65]
Soy hull	Langmuir	7.29	[67]
Sugarcane bagasse–lemongrass blend	Freundlich	1.4397 (Langmuir)	[13]
Sugarcane bagasse–lemongrass blend	Toth	0.91	This study

In the MOORA method, performance values are converted into a common normalized scale. MOORA is recognized for being both straightforward and computationally light in its approach. The use of MOORA evades the utilization complexities of pairwise evaluations or distance-based calculations in the traditional popular method. Through the application of normalization, MOORA can compare efficiently the diverse criteria expressed in different units. MOORA falls under the umbrella of MCDM or Multi-criteria decision-making techniques. It has been widely applied to rank competing models, such as in the evaluation of Software Reliability Growth Models (SRGMs), and has only recently been applied to biosorption [52] and biodegradation [68].

The MOORA score for the Hill and Sips models yields identical values, and this reinforces the notion that the two models are numerically equivalent [51]. A notable constraint of nonlinear modelling, as in this study, is that limited datasets may inadequately represent adsorption behavior, as discussed above. To address these limitations, resampling techniques such as parametric bootstrapping [69], Monte Carlo simulations, and sensitivity analysis can be employed to enhance model robustness, leading to greater insight into adsorption behavior [70].

Toth

The Toth isotherm is a three-parameter model that captures adsorption on energetically heterogeneous surfaces, and preserves the correct low- and high-concentration limits. In the equation, t quantifies heterogeneity, and a smaller t value indicates stronger heterogeneity, while t→1 results in the Langmuir isotherm. The model remains physically meaningful over wide ranges. The model also reproduces Henry's law at low C_e values. Toth frequently outperforms Langmuir and Sips for dyes and organics in several studies 75], which reflects the model's ability to accommodate broad site-energy distributions.

At the same time, the models maintain the monolayer capacity approach.

Fritz-Schlunder III Model

The Fritz-Schlunder III model is specifically designed to describe multilayer adsorption, coupled with interactions between adsorbed molecules on heterogeneous surfaces. This model considers the possibility of multilayer adsorption at higher concentrations, with q_{mFS}, $K_{FS,}$ and nF_S being constants that describe the maximum adsorption capacity, the affinity of the binding sites, and the interactions between adsorbed molecules, respectively. The model aims to provide a more generalized and flexible approach to adsorption isotherms, capable of describing a wider range of adsorption phenomena than the Langmuir model. The Fritz-Schlunder III model, by including a quadratic term in the denominator, explicitly accounts for multilayer adsorption and interactions among adsorbed molecules. The Fritz-Schlunder III model is particularly useful for systems where multilayer adsorption and molecule-molecule interactions are important.

Langmuir isotherm

The Langmuir isotherm describes monolayer adsorption of an adsorbate onto a homogeneous adsorbent surface, assuming the adsorbent has a uniform structure, where all adsorption sites are identical and have the same energy [71]. The isotherm model is related to Henry's law but is distinct from its foundational principles. It is postulated that no further adsorption can occur at those sites once a single layer of adsorbate molecules has fully covered the surface [72]. The model has been successfully utilized as the best model for modeling equilibrium adsorption of chromium onto adsorbents [73–86].

Freundlich isotherm

The Freundlich isotherm model is an empirical equation that offers a more flexible approach to describing adsorption phenomena. The model represents a heterogeneous adsorbent surface where adsorption occurs across multiple layers [87,88]. The Freundlich isotherm, unlike the Langmuir isotherm, accounts for variations in adsorption site affinities and the potential for multilayer adsorption. The Freundlich equation is limited in its inability to predict the maximum possible adsorption [89]. Estimation of the maximum adsorption can be carried out using the Halsey rearrangement by leveraging the last C_e data point as an approximation for the maximum adsorption capacity.

CONCLUSION

Using various modeling exercises, coupled with numerous error functions and MOORA, the adsorption of Cr(VI) onto a sugarcane bagasse–lemongrass blend has demonstrated characteristics that are consistent with monolayer behavior and fits the Toth model well. The saturation of adsorption capacity at high equilibrium concentrations is a testament to this. This study leverages the use of nonlinear regression instead of the often-popular linearized forms. In this manner, the study has provided accurate fits for most models, with 95% confidence interval output. The MOORA method for ranking models introduces a structured, unbiased ranking approach and effectively manages the multiple error criteria utilized in this study. Despite this, which is reiterated in several previous studies, the small dataset size remains a limitation. This limitation may introduce statistical noise and result in wide confidence intervals, which can compromise the estimation of the parameters. Future studies are encouraged to incorporate larger datasets to prevent this issue, preferably larger than 15. The use of resampling techniques such as bootstrapping or Monte Carlo simulation, which can enhance robustness, is also recommended. To conclude, this study supports the suitability of Langmuir-like isotherms for Cr(VI) adsorption onto a sugarcane bagasse–lemongrass blend and also validates MOORA as a valuable tool in adsorption model selection.

REFERENCES

1. Tumolo M, Ancona V, De Paola D, Losacco D, Campanale C, Massarelli C, et al. Chromium Pollution in European Water, Sources, Health Risk, and Remediation Strategies: An Overview. International Journal of Environmental Research and Public Health. 2020 Jan;17(15):5438.
2. Prasad S, Yadav KK, Kumar S, Gupta N, Cabral-Pinto MMS, Rezania S, et al. Chromium contamination and effect on environmental health and its remediation: A sustainable approaches. Journal of Environmental Management. 2021 May 1;285:112174.
3. Mohammadpour A, Gharehchahi E, Gharaghani MA, Shahsavani E, Golaki M, Berndtsson R, et al. Assessment of drinking water quality and identifying pollution sources in a chromite mining region. Journal of Hazardous Materials. 2024 Dec 5;480:136050.
4. Chaudhuri M, Azizan NKB. Adsorptive Removal of Chromium(VI) from Aqueous Solution by an Agricultural Waste-Based Activated Carbon. Water Air Soil Pollut. 2012 May 1;223(4):1765–71.
5. Amir A, Rahim R, Abdul-Talib S. Removal of Chromium Hexavalent Using Agriculture Waste. International Journal of Environmental Science and Development. 2017 Jan 1;8:260–3.
6. Hanafiah SFM, Salleh NFM, Ghafar NA, Shukri NM, Kamarudin NHN, Hapani M, et al. Efficiency of Coconut Husk as Agricultural Adsorbent in Removal of Chromium and Nickel Ions from Aqueous Solution. IOP Conf Ser: Earth Environ Sci. 2020 Dec;596(1):012048.
7. Konradt N, Dillmann S, Becker J, Schroden D, Rohns HP, Wagner C, et al. Removal of Chromium Species from Low-Contaminated Raw Water by Different Drinking Water Treatment Processes. Water. 2023 Jan;15(3):516.
8. Singh VP, Godara P, Srivastava A. Sustainable microalgal bioremediation of heavy metals and dyes from synthetic wastewater: Progressing towards United Nations Sustainable Development Goals. Waste Management Bulletin. 2024 Dec 1;2(4):123–35.
9. Meftah S, Meftah K, Drissi M, Radah I, Malous K, Amahrous A, et al. Heavy metal polluted water: Effects and sustainable treatment solutions using bio-adsorbents aligned with the SDGs. Discov Sustain. 2025 Feb 25;6(1):137.
10. Foo LPY, Tee CZ, Raimy NR, Hassell DG, Lee LY. Potential Malaysia agricultural waste materials for the biosorption of cadmium(II) from aqueous solution. Clean Techn Environ Policy. 2012 Apr 1;14(2):273–80.
11. Khan T, Isa MH, Mustafa MRU, Yeek-Chia H, Baloo L, Manan TSBA, et al. Cr(VI) adsorption from aqueous solution by an agricultural waste based carbon. RSC Adv. 2016 June 9;6(61):56365–74.
12. Khalifa MAS, Malek NANN, Farimani AY, Sani NS, Kamaru AA. Cetylpyridinium bromide (CPB)-treated sugarcane bagasse for the removal of chromate in aqueous solution. Materials Today: Proceedings. 2021 Jan 1;47:1252–7.
13. Aminu Dangamba S, Oyegoke T, Ocheje F, Aminu Dikko M, Galadima M. Evaluating the Adsorption Potential of Sugarcane Bagasse and Lemongrass for Chromium (VI) Removal in Wastewater Treatment. Journal of Engineering Science. 2024 Nov 20;31:96–116.
14. Garg UK, Kaur MP, Garg VK, Sud D. Removal of hexavalent chromium from aqueous solution by agricultural waste biomass. J Hazard Mater. 2007 Feb 9;140(1–2):60–8.
15. Vijayaraghavan K, Joshi UM, Balasubramanian R. Removal of metal ions from storm-water runoff by low-cost sorbents: Batch and column studies. Journal of Environmental Engineering. 2010;136(10):1113–8.

16. Mesfin Yeneneh A, Maitra S, Eldemerdash U. Study on biosorption of heavy metals by modified lignocellulosic waste. Journal of Applied Sciences. 2011;11(21):3555–62.
17. Dos Santos VCG, Salvado ADPA, Dragunski DC, Peraro DNC, Tarley CRT, Caetano J. Highly improved chromium (III) uptake capacity in modified sugarcane bagasse using different chemical treatments. Quimica Nova. 2012;35(8):1606–11.
18. Ullah I, Nadeem R, Iqbal M, Manzoor Q. Biosorption of chromium onto native and immobilized sugarcane bagasse waste biomass. Ecological Engineering. 2013;60:99–107.
19. Sadaf S, Bhatti HN, Nausheen S, Noreen S. Potential use of low-cost lignocellulosic waste for the removal of direct violet 51 from aqueous solution: Equilibrium and breakthrough studies. Archives of Environmental Contamination and Toxicology. 2014;66(4):557–71.
20. Mahmood-ul-Hassan M, Suthar V, Rafique E, Ahmad R, Yasin M. Kinetics of cadmium, chromium, and lead sorption onto chemically modified sugarcane bagasse and wheat straw. Environ Monit Assess. 2015 June 27;187(7):470.
21. Tawfik GM, Dila KAS, Mohamed MYF, Tam DNH, Kien ND, Ahmed AM, et al. A step by step guide for conducting a systematic review and meta-analysis with simulation data. Tropical Medicine and Health. 2019 Aug 1;47(1):46.
22. Khare KS, Phelan FR. Quantitative Comparison of Atomistic Simulations with Experiment for a Cross-Linked Epoxy: A Specific Volume-Cooling Rate Analysis. Macromolecules. 2018;51(2):564–75.
23. Langmuir I. THE ADSORPTION OF GASES ON PLANE SURFACES OF GLASS, MICA AND PLATINUM. Journal of the American Chemical Society. 1918;40(2):1361–402.
24. Schirmer W. Physical Chemistry of Surfaces. Zeitschrift für Physikalische Chemie. 1999;210(1):134–5.
25. Ridha FN, Webley PA. Anomalous Henry's law behavior of nitrogen and carbon dioxide adsorption on alkali-exchanged chabazite zeolites. Separation and Purification Technology. 2009;67(3):336–43.
26. Jovanović DS. Physical adsorption of gases - I: Isotherms for monolayer and multilayer adsorption. Kolloid-Zeitschrift & Zeitschrift für Polymere. 1969;235(1):1203–13.
27. Carmo AM, Hundal LS, Thompson ML. Sorption of hydrophobic organic compounds by soil materials: Application of unit equivalent Freundlich coefficients. Environmental Science and Technology. 2000;34(20):4363–9.
28. Radushkevich LV. Potential theory of sorption and structure of carbons. Zhurnal Fizicheskoi Khimii. 1949;23:1410–20.
29. Dubinin MM. Modern state of the theory of volume filling of micropore adsorbents during adsorption of gases and steams on carbon adsorbents. Zh Fiz Khim. 1965;39(6):1305–17.
30. Mahanty B, Behera SK, Sahoo NK. Misinterpretation of Dubinin–Radushkevich isotherm and its implications on adsorption parameter estimates. Separation Science and Technology. 2023 May 3;58(7):1275–82.
31. Mudhoo A, Pittman CU. The Dubinin-Radushkevich models: Dissecting the *ps*/*p* to *cs*/*ce* replacement in solid-aqueous interfacial adsorption and tracking the validity of $E = 8$ kJ mol–1 for assigning sorption type. Chemical Engineering Research and Design. 2023 Oct 1;198:370–402.
32. Koble RA, Corrigan TE. Adsorption isotherms for pure hydrocarbons. Ind Eng Chem. 1952 Feb 1;44(2):383–7.
33. Temkin MI, Pyzhev V. Kinetics of ammonia synthesis on promoted iron catalysts. Acta Physicochim USSR. 1940;12(3):327–56.
34. Chu KH. Revisiting the Temkin Isotherm: Dimensional Inconsistency and Approximate Forms. Industrial & Engineering Chemistry Research [Internet]. 2021 Aug 16 [cited 2022 Sept 1]; Available from: https://pubs.acs.org/doi/pdf/10.1021/acs.iecr.1c01788
35. Redlich O, Peterson DL. A Useful Adsorption Isotherm. Shell Development Company, Emeryville, California. 1958;63:1024.
36. Sips R. On the structure of a catalyst surface. The Journal of Chemical Physics. 1948;16(5):490–5.
37. Tóth J. Uniform interpretation of gas/solid adsorption. Advances in Colloid and Interface Science. 1995;55(C):1–239.
38. Hill AV. The possible effects of the aggregation of the molecules of haemoglobin on its dissociation curves. J Physiol. 1910;40:iv–vii.
39. Khan AA, Singh RP. Adsorption thermodynamics of carbofuran on Sn (IV) arsenosilicate in H+, Na+ and Ca2+ forms. Colloids and Surfaces. 1987;24(1):33–42.
40. Brunauer S, Emmett PH, Teller E. Adsorption of Gases in Multimolecular Layers. Journal of the American Chemical Society. 1938;60(2):309–19.
41. Vieth WR, Sladek KJ. A model for diffusion in a glassy polymer. Journal of Colloid Science. 1965;20(9):1014–33.
42. Radke CJ, Prausnitz JM. Adsorption of Organic Solutes from Dilute Aqueous Solution of Activated Carbon. Journal of the American Chemical Society. 1972;11(4):445–51.
43. Liu Y, Liu YJ. Biosorption isotherms, kinetics and thermodynamics. Separation and Purification Technology. 2008;61(3):229–42.
44. Tran HN, Bollinger JC, Lima EC, Juang RS. How to avoid mistakes in treating adsorption isotherm data (liquid and solid phases): Some comments about correctly using Radke-Prausnitz nonlinear model and Langmuir equilibrium constant. J Environ Manage. 2023 Jan 1;325(Pt A):116475.
45. Brouers F, Sotolongo O, Marquez F, Pirard JP. Microporous and heterogeneous surface adsorption isotherms arising from Levy distributions. Physica A: Statistical Mechanics and its Applications. 2005 Apr 1;349(1):271–82.
46. Hamissa AMB, Brouers F, Mahjoub B, Seffen M. Adsorption of Textile Dyes Using Agave Americana (L.) Fibres: Equilibrium and Kinetics Modelling. Adsorption Science & Technology. 2007 June 1;25(5):311–25.
47. Brouers F, Al-Musawi TJ. Brouers-Sotolongo fractal kinetics versus fractional derivative kinetics: A new strategy to analyze the pollutants sorption kinetics in porous materials. Journal of Hazardous Materials. 2018 May 15;350:162–8.
48. Fritz W, Schluender EU. Simultaneous adsorption equilibria of organic solutes in dilute aqueous solutions on activated carbon. Chemical Engineering Science. 1974;29(5):1279–82.
49. Chu KH, Tan B. Is the Frumkin (Fowler–Guggenheim) adsorption isotherm a two- or three-parameter equation? Colloid and Interface Science Communications. 2021 Nov 1;45:100519.
50. Martucci A, Braschi I, Bisio C, Sarti E, Rodeghero E, Bagatin R, et al. Influence of water on the retention of methyl tertiary-butyl ether by high silica ZSM-5 and Y zeolites: A multidisciplinary study on the adsorption from liquid and gas phase. RSC Advances. 2015;5(106):86997–7006.
51. Chu KH, Debord J, Harel M, Bollinger JC. Mirror, Mirror on the Wall, Which Is the Fairest of Them All? Comparing the Hill, Sips, Koble–Corrigan, and Liu Adsorption Isotherms. Ind Eng Chem Res. 2022 May 18;61(19):6781–90.
52. Shukor MY. Chitosan–Silica Composite Aerogel for the Adsorption of Cupric Ions: Isothermal Remodeling and MOORA-Based Model Selection. Journal of Environmental Microbiology and Toxicology. 2024 Dec 26;12(2):53–62.
53. Hannan EJ, Quinn BG. The Determination of the Order of an Autoregression. Journal of the Royal Statistical Society: Series B (Methodological). 1979;41(2):190–5.
54. Ross T. Indices for performance evaluation of predictive models in food microbiology. Journal of Applied Bacteriology. 1996;81(5):501–8.
55. Ezekiel M. The Sampling Variability of Linear and Curvilinear Regressions: A First Approximation to the Reliability of the Results Secured by the Graphic 'Successive Approximation' Method. The Annals of Mathematical Statistics. 1930;1(4):275–333.
56. Akaike H. A New Look at the Statistical Model Identification. IEEE Transactions on Automatic Control. 1974;19(6):716–23.
57. Burnham KP, Anderson DR. Multimodel inference: Understanding AIC and BIC in model selection. Sociological Methods and Research. 2004;33(2):261–304.
58. Marquardt DW. An Algorithm for Least-Squares Estimation of Nonlinear Parameters. Journal of the Society for Industrial and Applied Mathematics. 1963;11(2):431–41.
59. Seidel A, Gelbin D. On applying the ideal adsorbed solution theory to multicomponent adsorption equilibria of dissolved organic components on activated carbon. Chemical Engineering Science. 1988 Jan 1;43(1):79–88.
60. Porter JF, McKay G, Choy KH. The prediction of sorption from a binary mixture of acidic dyes using single- and mixed-isotherm

variants of the ideal adsorbed solute theory. Chemical Engineering Science. 1999;54(24):5863–85.
61. Schwarz G. Estimating the Dimension of a Model. The Annals of Statistics. 1978;6(2):461–4.
62. Motulsky HJ, Ransnas LA. Fitting curves to data using nonlinear regression: a practical and nonmathematical review. The FASEB Journal. 1987;1(5):365–74.
63. Prasanthi MR, Jayasravanthi M, Nadh RV. Kinetic, thermodynamic and equilibrium studies on removal of hexavalent chromium from aqueous solutions using agro-waste biomaterials, casuarina equisetifolia L. and sorghum bicolor. Korean Journal of Chemical Engineering. 2016;33(8):2374–83.
64. Rzig B, Guesmi F, Sillanpää M, Hamrouni B. Biosorption potential of olive leaves as a novel low-cost adsorbent for the removal of hexavalent chromium from wastewater. Biomass Conv Bioref. 2024 June 1;14(12):12961–79.
65. Ayele AL, Tizazu BZ, Wassie AB. Chemical Modification of Teff Straw Biomass for Adsorptive Removal of Cr (VI) from Aqueous Solution: Characterization, Optimization, Kinetics, and Thermodynamic Aspects. Adsorption Science & Technology [Internet]. 2022 Apr 15 [cited 2024 Sept 20]; Available from: https://journals.sagepub.com/doi/full/10.1155/2022/5820207
66. Kumar P, Chauhan MS. Adsorption of chromium (VI) from the synthetic aqueous solution using chemically modified dried water hyacinth roots. Journal of Environmental Chemical Engineering. 2019 Aug;7(4):103218.
67. Blanes PS, Bordoni ME, González JC, García SI, Atria AM, Sala LF, et al. Application of soy hull biomass in removal of Cr(VI) from contaminated waters. Kinetic, thermodynamic and continuous sorption studies. Journal of Environmental Chemical Engineering. 2016 Mar 1;4(1):516–26.
68. Halmi MIE, Syed MA, Shamaan NA, Shukor MY. Mathematical Modeling of Molybdenum Reduction to Molybdenum Blue by Burkholderia sp. Strain Dr.Y27 and Model Selection Using the MOORA Method. Journal of Environmental Bioremediation and Toxicology. 2024 Dec 26;7(2):17–24.
69. Efron B. Bootstrap Methods: Another Look at the Jackknife. Ann Statist. 1979 Jan;7(1):1–26.
70. Lambert RJW, Mytilinaios I, Maitland L, Brown AM. Monte Carlo simulation of parameter confidence intervals for non-linear regression analysis of biological data using Microsoft Excel. Computer Methods and Programs in Biomedicine. 2012 Aug 1;107(2):155–63.
71. Langmuir I. The constitution and fundamental properties of solids and liquids. Part I. Solids. Journal of the American Chemical Society. 1916;38(11):2221–95.
72. Foo KY, Hameed BH. Insights into the modeling of adsorption isotherm systems. Chemical Engineering Journal. 2010;156(1):2–10.
73. Karnib M, Kabbani A, Holail H, Olama Z. Heavy Metals Removal Using Activated Carbon, Silica and Silica Activated Carbon Composite. Energy Procedia. 2014 Dec 31;50:113–20.
74. Hyder AHMG, Begum SA, Egiebor NO. Adsorption isotherm and kinetic studies of hexavalent chromium removal from aqueous solution onto bone char. Journal of Environmental Chemical Engineering. 2015 June 1;3(2):1329–36.
75. Divband Hafshejani L, Mortazavi P, Sabz ALiPour S, Brooman Nasab S. Isotherm and Kinetics Study of The Adsorption of Chromium (VI) From Aqueous Solution by Zizyphus Spina-christi Leaves Ash Nanoparticles. Irrigation Sciences and Engineering. 2016 Dec 21;39(4):97–110.
76. Taha AA, Shreadah MA, Ahmed AM, Heiba HF. Multi-component adsorption of Pb(II), Cd(II), and Ni(II) onto Egyptian Na-activated bentonite; Equilibrium, kinetics, thermodynamics, and application for seawater desalination. Journal of Environmental Chemical Engineering. 2016;4(1):1166–80.
77. Nag S, Mondal A, Bar N, Das SK. Biosorption of chromium (VI) from aqueous solutions and ANN modelling. Environ Sci Pollut Res. 2017 Aug 1;24(23):18817–35.
78. Srivastava S, Agrawal SB, Mondal MK. Synthesis, characterization and application of Lagerstroemia speciosa embedded magnetic nanoparticle for Cr(VI) adsorption from aqueous solution. J Environ Sci (China). 2017 May;55:283–93.
79. Ahsan MdA, Jabbari V, Islam MdT, Kim H, Hernandez-Viezcas JA, Lin Y, et al. Green synthesis of a highly efficient biosorbent for organic, pharmaceutical, and heavy metal pollutants removal: Engineering surface chemistry of polymeric biomass of spent coffee waste. Journal of Water Process Engineering. 2018 Oct 1;25:309–19.
80. Boeykens SP, Saralegui A, Caracciolo N, Piol MN. Agroindustrial waste for lead and chromium biosorption. Journal of Sustainable Development of Energy, Water and Environment Systems. 2018;6(2):341–50.
81. Mahmood-Ul-Hassan M, Suthar V, Ahmad R, Yousra M. Biosorption of metal ions on lignocellulosic materials: batch and continuous-flow process studies. Environmental Monitoring and Assessment. 2018;190(5).
82. Mortazavian S, An H, Chun D, Moon J. Activated carbon impregnated by zero-valent iron nanoparticles (AC/nZVI) optimized for simultaneous adsorption and reduction of aqueous hexavalent chromium: Material characterizations and kinetic studies. Chemical Engineering Journal. 2018 July 1;353.
83. Sadiq A, Choubey A, Bajpai AK, Sadiq A, Choubey A, Bajpai AK. Biosorption of chromium ions by calcium alginate nanoparticles. Journal of the Chilean Chemical Society. 2018;63(3):4077–81.
84. Abilio TE, Soares BC, José JC, Milani PA, Labuto G, Carrilho ENVM. Hexavalent chromium removal from water: adsorption properties of in natura and magnetic nanomodified sugarcane bagasse. Environmental Science and Pollution Research. 2021;28(19):24816–29.
85. Dan-Iya BI, Shukor MY. Isothermal Modelling of the Adsorption of Chromium onto Calcium Alginate Nanoparticles. Journal of Environmental Microbiology and Toxicology. 2021 Dec 31;9(2):1–7.
86. Mahmoud ME, El-Said GF, Ibrahim GAA, Elnashar AAS. Effective removal of hexavalent chromium from water by sustainable nano-scaled waste avocado seeds: adsorption isotherm, thermodynamics, kinetics, and error function. Biomass Conversion and Biorefinery [Internet]. 2022; Available from: https://www.scopus.com/inward/record.uri?eid=2-s2.0-85144861871&doi=10.1007%2fs13399-022-03619-2&partnerID=40&md5=92f885dfde215c605d5baa0cebf9b79c
87. Freundlich H. Über die adsorption in lösungen (Over the adsorption in solution). Zeitschrift für Physikalische Chemie. 1907;57(1):385–470.
88. Rushton G, Karns C, Shimizu K. A critical examination of the use of the Freundlich isotherm in characterizing molecularly imprinted polymers (MIPs). Analytica Chimica Acta. 2005 Jan 3;528:107–13.
89. Ahmed S, Guo Y, Li D, Tang P, Feng Y. Superb removal capacity of hierarchically porous magnesium oxide for phosphate and methyl orange. Environ Sci Pollut Res. 2018 Sept 1;25(25):24907–16.